Enhanced Performance of a Self-Powered ZnO Photodetector by Coupling LSPR-Inspired Pyro-Phototronic Effect and Piezo-Phototronic Effect

Qi Li, Jing Huang, Jianping Meng,* and Zhou Li*

Ultraviolet detection is overriding priority in many military and civilian fields. A photodetector can be effectively enhanced by introducing piezo-phototronic effect, pyro-phototronic effect, and localized surface plasmon resonance (LSPR). Coupling piezo-phototronic, pyro-phototronic, and LSPR effect can be realized in a self-powered photodetector based on ZnO/CuO nanorods covered with Au nanoparticles (NPs). The influences of LSPR, pyroelectric and external pressure on the performance of devices are thoroughly investigated, respectively. ZnO/CuO/Au devices display the most attractive performance under pressure of 73.7 N. The maxima of responsivity and detectivity are obtained as 0.81 mA W^{-1} and 3.3 × 10^{13} Jones, respectively, under pressure of 73.7 N when detecting weak ultraviolet radiation (140 nW cm^{-2}). Responsivity and detectivity are dramatically enhanced by 17× and 12× compared to CuO/ZnO devices. Moreover, rise time and fall time reduce from 114/75 ms of a ZnO/CuO device to 18/12 ms of a ZnO/CuO/Au device under pressure of 64.7 N. These results demonstrate that LSPR, pyro-phototronic, and piezo-phototronic coupled effect makes greater improvement than the individual effects in the performance of photodetectors. This work probably can be a cornerstone of designing high-performance photodetectors using other nanomaterial systems as well.

1. Introduction

Human beings expose to ultraviolet usually and utilize ultraviolet to make a better life such as sterilization and flame sensing. Thus, precise sensing of ultraviolet, especially weak ultraviolet, is of great importance to take advantage of invisible ultraviolet light safely and reliably.[1] The performance of a photodetector is strongly dependent on sensing materials. ZnO, a wide bandgap semiconductor (3.37 eV), possesses large exciton binding energy (≈60 meV), at room temperature and is an environmentally-friendly material that is tolerant of chemicals and radiation.[2–5] Accordingly, ZnO is an excellent candidate for manufacturing UV photodetectors. However, ZnO-based photodetectors are still confronted with the low responsivity for UV light with low power density. Furthermore, there is also some weakness for fabricating ZnO-based photodetectors. For example, persistent photoconductivity (PPC) prolongs the recovery time noticeably owing to inherent oxygen vacancies in ZnO.[6,7] To solve those issues above mentioned are beneficial to constructing high performance ZnO-based photodetectors that have high responsivity, high detectivity, and fast response and recovery.

Two strategies, including piezoelectric effect and pyroelectric effect, are used to address the above issues. Piezoelectric effect and pyroelectric effect are inherent characteristics of ZnO, owing to the noncentral-symmetric crystal structure.[8,9] Piezoelectric polarization charges within the interface are able to modulate the charge carriers' separation and recombination effectively.[10] This phenomenon is known as the piezo-phototronic effect and can be used to promote the performance of ZnO-based photodetectors such as sensitivity and responsivity.[11–14] Photothermal conversion in ZnO will contribute to pyroelectric effect during illumination. Hence, pyro-phototronic effect is also utilized to develop ZnO photodetectors, for combining pyroelectric effect and photoexcitation effect.[2,15–17] Coupling pyro-phototronic effect and piezo-phototronic effect is an useful method to further improve performance of ZnO-based photodetectors.[18–20] Because pyroelectric and piezoelectric effects are both based on the polarization charges generated

Q. Li, J. Huang, Z. Li
College of Chemistry and Chemical Engineering
Center on Nanoenergy Research
Guangxi University
Nanning 530004, China
E-mail: zli@binn.cas.cn

Q. Li, J. Huang, J. Meng, Z. Li
CAS Center for Excellence in Nanoscience
Beijing Key Laboratory of Micro-Nano Energy and Sensor
Beijing Institute of Nanoenergy and Nanosystems
Chinese Academy of Sciences
Beijing 101400, China
E-mail: mengjianping@binn.cas.cn

J. Meng, Z. Li
School of Nanoscience and Technology
University of Chinese Academy of Sciences
Beijing 100049, China

The ORCID identification number(s) for the author(s) of this article can be found under https://doi.org/10.1002/adom.202102468.

in ZnO semiconductor material along *c*-axis. Moreover, weak ultraviolet cannot lead to strong enough pyroelectric current for a little temperature change. Rising of the temperature variation at an instant of light illumination can enhance the performance of a photodetector based on the mechanism of pyro-phototronic effect.[21] Exactly, localized surface plasmon resonance (LSPR) of metal/compound nanoparticles (NPs) can produce much transient thermal power that can cooperate with the pyro-phototronic effect as the pyroelectric current can be enhanced by the significant increase of temperature from the transient thermal energy.[22–24] Our previous work has demonstrated that the LSPR-inspired pyro-phototronic effect can dramatically improve the performance of a photodetector.[25] It is significant to couple three work mechanisms including LSPR, pyro-phototronic, and piezo-phototronic. Because the coupled effect may further facilitate the improvement of ZnO-based photodetectors. More importantly, the relationship and interaction can be explored among the LSPR, pyro-phototronic, and piezo-phototronic in detail. Meanwhile, self-powered photodetectors without external power supply are one of the key optoelectronic devices when humans are subject to energy crisis.

In this paper, a strategy was proposed to couple the LSPR, pyro-phototronic, and piezo-phototronic effect and the interaction among them was studied. A self-powered photodetector based on p-n junction of p-CuO and n-ZnO was designed to demonstrate the coupled effect of LSPR, pyro-phototronic, and piezo-phototronic effect. The three effects can cooperate with each other well and enhance the performance of the photodetector. For the low power density of 140 nW cm^{-2}, the photocurrent can be improved by ≈523% via the LSPR-inspired pyro-phototronic effect. Further, by introducing a pressure of 73.7 N to the photodetector, the enhancement of photocurrent can be increased to over 2900%.

2. Results and Discussions

A schematic illustration of the device structure was shown in **Figure 1**a and the fabricating process detailed in the experimental section. A ZnO seed layer was deposited on the substrate and then a hydrothermal method was utilized to grow ZnO nanorods. A thin CuO shell covered the ZnO nanorods by a solution-based method. Lastly, Au NPs were decorated on each CuO-coated ZnO nanorod and then FTO covered the top of the devices as a top electrode to produce ZnO/CuO/Au photodetectors. The ZnO/CuO devices were obtained by the same method except for sputtering Au NPs. The single nanorod of ZnO/CuO/Au (Figure 1b) showed many particles and a rough surface, which indicated the ZnO was covered by the CuO shell and Au NPs. The SEM (scanning electron microscope) image for ZnO/CuO/Au materials showed vertically aligned nanorods (Figures S1 and S2a, Supporting Information). Further proof
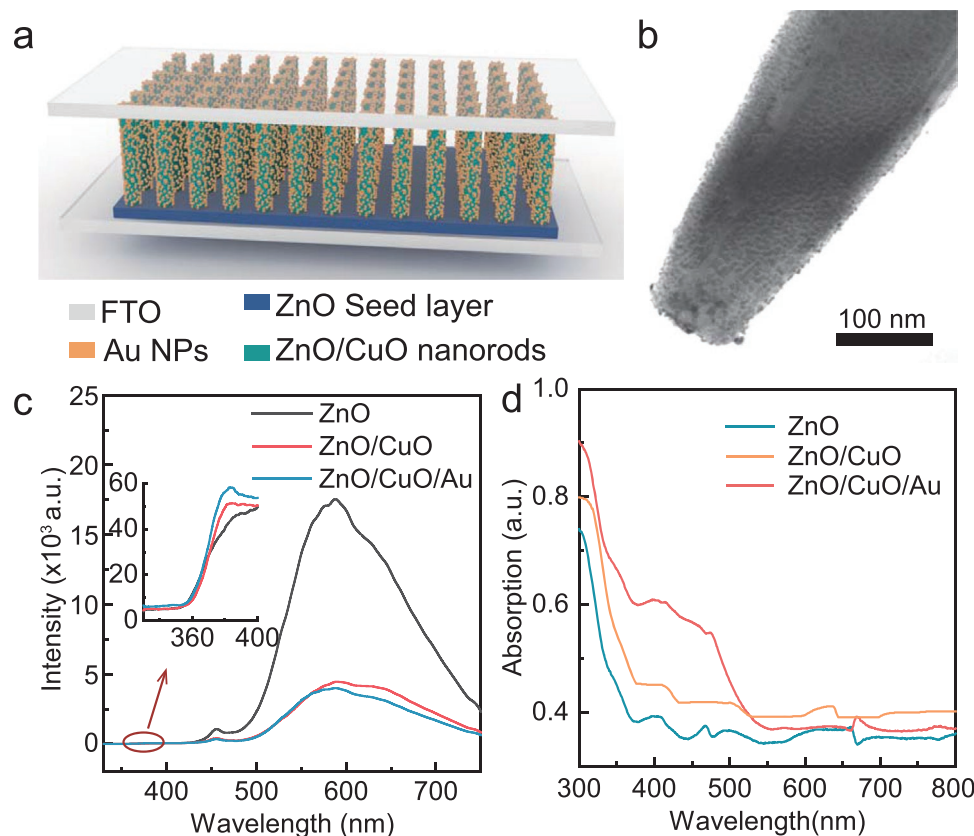

Figure 1. Device structure and basic characterization of the self-powered p-CuO/n-ZnO/Au NPs photodetector. a) Device structures of the photodetectors. b) A TEM image of a single ZnO/CuO/Au nanorod. c) Photoluminescence spectra for ZnO, ZnO/CuO, and ZnO/CuO/Au. d) UV–vis–NIR absorption spectra of ZnO, ZnO/CuO, and ZnO/CuO/Au.
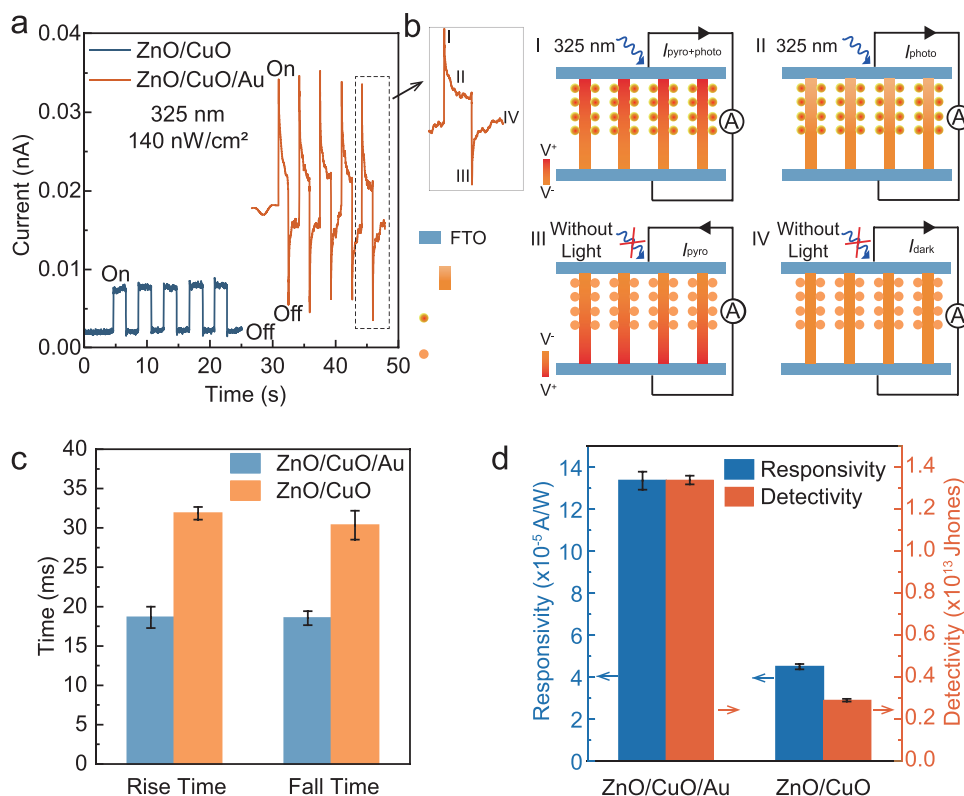
Figure 2. LSPR contributed to the pyroelectric effect in ZnO/CuO/Au photodetectors. a) Transient I–t characteristics of ZnO/CuO and ZnO/CuO/Au devices (free from pressure) under illumination of 325 nm UV laser (140 nW cm^{-2}) and zero bias. b) Systematical illustration of the typic four-steps photoresponse of a complete pyro-phototronic effect inspired by LSPR of Au NPs. c) Response time of the photodetectors decreased by coupled LSPR and pyroelectric effect under 325 nm illumination (140 nW cm^{-2}). d) Responsivity and detectivity enhanced by coupled LSPR and pyroelectric effect under 325 nm illumination (140 nW cm^{-2}).

can be found in the high-resolution TEM (transmission electron microscope) and corresponding elements distribution confirmed by EDS (energy dispersive spectroscopy) spectrum. The high-resolution TEM and corresponding elements distribution confirmed by EDS indicated the existence of Au, Cu, O, Zn (Figure S2b–e, Supporting Information). Detailed Au NP morphology was confirmed by high-resolution TEM (Figure S3, Supporting Information). The size of Au NPs approached 3 nm. Photoluminescence spectra for ZnO, ZnO/CuO and ZnO/CuO/Au (Figure 1c) displayed inherent emission at around 380 nm, visible luminescence at 456 nm and broad visible luminescence from 500 to 700 nm. The visible luminescence indicated various deep level defects such as oxygen interstitials and oxygen vacancies and surface states in ZnO.[26] Furthermore, the visible luminescence was suppressed for ZnO/CuO and ZnO/CuO/Au. There were three reasons for that.[27–30] 1) CuO led to a reduction of the surface traps due to screening effects. As a result, less holes were able to be captured at the surface traps, which quenched the visible emission. 2) Depletion in p-n junction will lead to competitive processes for activation and recombination of oxygen vacancies. 3) The density of surface defect states can be reduced via the surface passivation by CuO and Au NPs. Importantly, the hot holes generated by LSPR of Au NPs can recombine with the electrons present at the V_o^x, V_o^+ states. ZnO/CuO/Au exhibited considerable absorption in the UV range and the absorption was stronger than ZnO, which

was attributed to LSPR produced by Au NPs for the enhanced absorption of light and efficiency of photothermal conversion (Figure 1d).[31–33] The bandgaps of ZnO and CuO were calculated as 3.38 and 1.14 eV respectively (Figure S4, Supporting Information). Raman spectra of the ZnO/CuO/Au and X-ray diffractometer (XRD) for ZnO, ZnO/CuO, and ZnO/CuO/Au at room temperature pointed out that there were two components in the materials containing ZnO and CuO (Figure S5, Supporting Information). All of these results from materials characteristic indicated that ZnO/CuO/Au NPs nanorods were obtained by our easy method.

The excellent transient response of the photodetectors was obtained under illumination of a 325 nm laser (140 nW cm^{-2}) without external bias voltage (0 V). The pyroelectric current was observed for ZnO/CuO/Au devices but not for ZnO/CuO devices (**Figure 2**a). Because the current-time response of ZnO/CuO/Au devices displayed a typical four-stage dynamic photocurrent response caused by the recently invented pyro-phototronic effect,[34,35] which was systematically illustrated in Figure 2b. Consequently, LSPR generated by Au NPs inspired this pyro-phototronic effect at the moment of light illumination. We called this work mechanism the LSPR-inspired pyro-phototronic effect here. At first, the photodetector was under the initial dark condition showing dark current I_{dark}. When the photodetector was exposed to 325 nm laser, photo-generated electron–hole pairs were produced and then separated by the
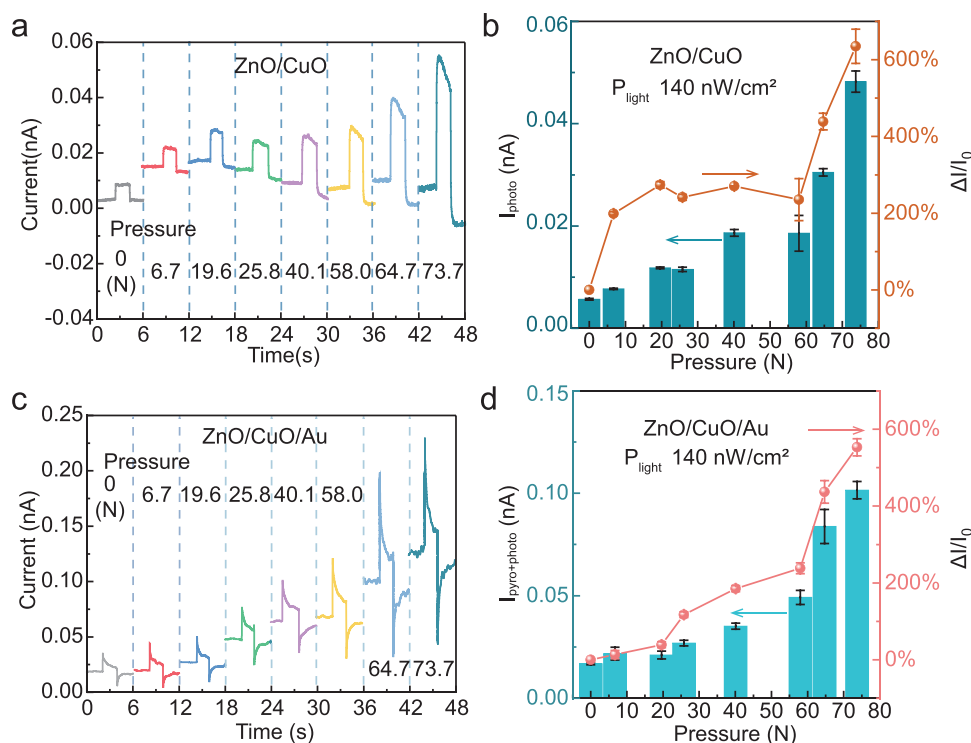
ADVANCED
SCIENCE NEWS
www.advancedsciencenews.com

ADVANCED
OPTICAL
MATERIALS
www.advopticalmat.de

Figure 3. Piezo-phototronic effect induced performance enhancement in the photodetectors. a) Transient I–t characteristics of ZnO/CuO devices under different external pressure from 0 to 73.7 N and b) corresponding photocurrent as well as relative change of $\Delta I/I_0$ under 325 nm illumination (140 nW cm^{-2}). c) Transient I–t characteristics of ZnO/CuO/Au devices under different external pressure from 0 to 73.7 N and d) corresponding photocurrent as well as relative change of $\Delta I/I_0$ under 325 nm illumination (140 nW cm^{-2}).

built-in field of p-n junction formed by ZnO and CuO,[36,37] and displayed a transient temperature increase of the ZnO nanorods for the mass heat from LSPR effect of Au NPs simultaneously (Figure 2b stage I). As a result, photocurrent I_{photo} and pyroelectric current displayed as a spike current $I_{pyro+photo}$. The temperature of the ZnO nanorods remained almost constant for the weak heating capability of ultraviolet and pyro-potentials in ZnO nanorods disappeared as there was no significant temperature change. Therefore, the spike current $I_{pyro+photo}$ fell off and reached a plateau showing as I_{photo} (Figure 2b stage II). The temperature of ZnO nanorods decreased immediately, resulting in opposite distribution of pyro-potentials. So, the reversed current I_{pyro} emerged (Figure 2b stage III). Finally, the temperature of the ZnO was steady and there was only dark current I_{dark} (Figure 2b stage IV). Performance of the photodetectors will be promoted by the LSPR-inspired pyro-phototronic effect. Rise time/fall time decreased from 30/31 ms of ZnO/CuO devices to 19/19 ms of ZnO/CuO/Au devices, which showed ≈30% reduction (Figure 2c). Responsivity (R) and detectivity (D^*) were used as important parameters to describe the sensitivity of a photodetector. Responsivity was calculated by $R = (I_{light} - I_{dark})/(SP)$ and detectivity was calculated by $D^* = R/(2q \cdot I_{dark}/S)^{0.5}$, where S, P, I_{light}, I_{dark}, and q were effective area of the photodetector, incident light power density, photocurrent, dark current, and the electron charge, respectively.[38] Transient R for ZnO/CuO/Au devices was 0.13 mA W^{-1} which was three times that of ZnO/CuO devices (0.046 mA W^{-1}) (Figure 2d). Transient D^* for ZnO/CuO/Au devices was 1.3×10^{13} Jones (cm Hz$^{1/2}$ W^{-1}) which was five times that of ZnO/CuO devices (2.9×10^{12}

Jones) (Figure 2d). The great improvement of performance for ZnO/CuO/Au devices indicated that LSPR induced by plasmonic Au NPs inspired the pyroelectric effect of ZnO, and the coupled LSPR effect and pyroelectric effect played a key role in the enhancement of the performance. Moreover, the ZnO/CuO devices still exhibited no pyroelectric under illumination of 365 nm light with high power density (50–200 µW cm^{-2}) and the devices displayed long recovery time for the increased power density of the incident light (Figure S6a, Supporting Information). However, the ZnO/CuO/Au devices showed the enhanced pyroelectric current and fast response as the power density of the incident light increased (Figure S6b, Supporting Information). Therefore, the results can further illustrate the importance of LSPR-inspired pyro-phototronic effect for the performance enhancement.

The piezo-phototronic effect was then investigated under illumination of a 325 nm laser (140 nW cm^{-2}) without external bias voltage (0 V) in the ZnO/CuO and ZnO/CuO/Au devices through time-dependent response under different pressure (**Figure 3**a,c). It was important to demonstrate that the contact resistance between materials and FTO electrodes will not decrease with increase of pressure. The I–V curves of ohmic-contacted ZnO devices (FTO-ZnO-FTO) indicated the resistance of devices did not reduce (Figure S7, Supporting Information), which excluded the possibility that the current enhancement attributed to improvements in contact under pressure. Schematic illustration for the experimental setup can be observed in Figure S8a, Supporting Information. For ZnO/CuO devices, they only displayed the feature of current without
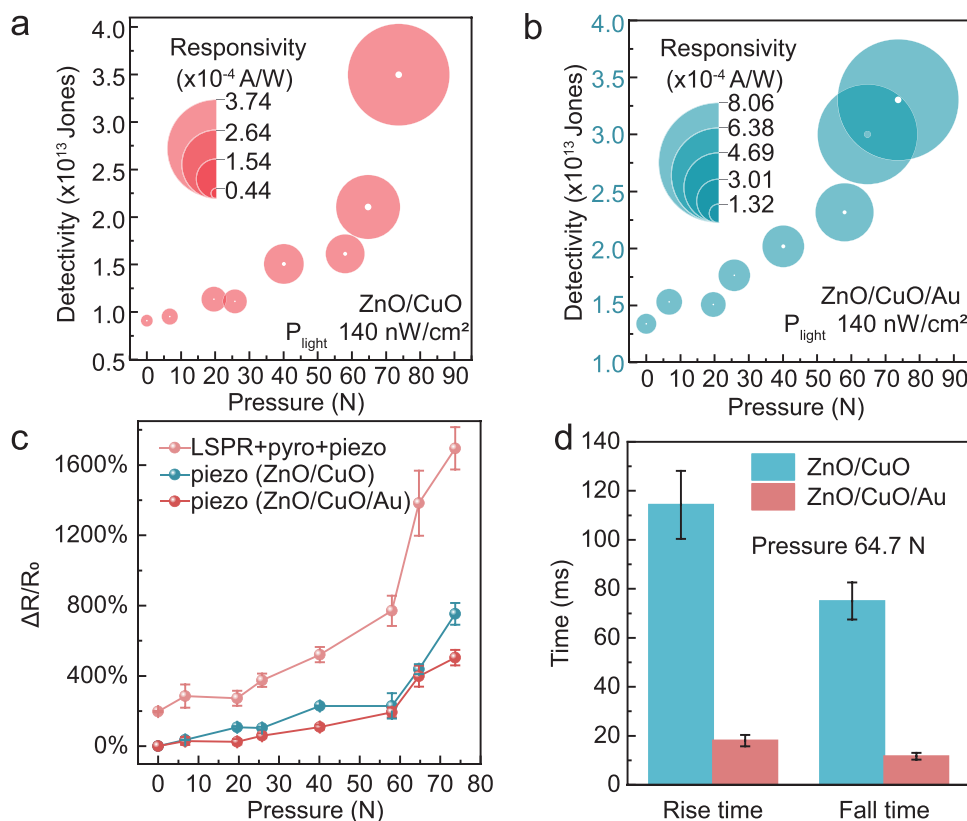
Figure 4. Influence of coupled LSPR-inspired pyro-phototronic effect and piezo-phototronic effect on performance of the ZnO-based photodetectors. a) Detectivity and responsivity for ZnO/CuO devices as a function of different applied pressure. b) Detectivity and responsivity for ZnO/CuO/Au devices as a function of different applied pressure. c) $\Delta R/R_0$ as a function of different applied pressure for quantitatively comparing the piezo-phototronic effect and the comprehensive effect induced responsivity. d) Response time decrease for coupled LSPR-inspired pyro-phototronic effect and piezo-phototronic effect.

spike current under different pressure from 0 to 73.7 N. The photocurrent I_{photo} ($I_{photo} = I_{light} - I_{dark}$) increased as the pressure rose up in general. The peak photocurrent was obtained as 0.048 nA at 73.7 N (Figure 3b). The figure of merit, $\Delta I/I_0$, was defined to achieve quantitative description of enhancement of piezo-phototronic effect. It was defined as $\Delta I/I_0 = (I - I_0)/I_0$, where I and I_0 were the light current under pressure and pressure free conditions, respectively. $\Delta I/I_0$ for ZnO/CuO device exhibited the trend of increase as the externally applied pressure rose up (Figure 3b). The maximum $\Delta I/I_0$ was 635% under pressure of 73.7 N, which suggested that photocurrent enhanced greatly by 635% for the piezo-phototronic effect playing a part. Unlike ZnO/CuO devices, ZnO/CuO/Au devices showed photocurrent $I_{pyro+photo}$ under different pressure from 0 to 73.7 N. The photocurrent grew monotonously as the pressure went up (Figure 3d). Maximum photocurrent was 0.10 nA under pressure of 73.7 N. Moreover, $\Delta I/I_0$ also exhibited the trend of increase as the externally applied pressure went up (Figure 3d) and reached maximum 553% under pressure of 73.7 N, which indicated that piezo-phototronic effect made light current enhance noticeably by 553%. The influences of the externally applied pressure on the charge carrier transport properties of the ZnO/CuO p-n junction were investigated by obtaining the I–V characteristics of the devices under UV illumination and dark condition (Figure S8b,c, Supporting

Information). It was obvious that the current/threshold voltage increased/decreased with pressure increased monotonously whatever the condition was UV or dark. Hence, barrier height of the p-n junction decreased as the pressure increased, indicating an effective modulation of the barrier height as well as the charge carrier transport properties through external pressure. The piezo-phototronic effect made a difference in performance of a photodetector under pressure, which was the same as the trends reported in previous works.[18,35,39,40]

The influences of the externally applied pressure on the performance of the self-powered ZnO-based photodetectors were investigated by calculating their detectivity and responsivity under different pressure. Responsivity and detectivity for ZnO/CuO devices displayed a growing trend with the increase of external pressure. The maximums of responsivity and detectivity were 0.38 mA W^{-1} and 3.5×10^{13} Jones respectively and all appeared at an externally applied pressure of 73.7 N (**Figure 4**a). The detectivity increased from 0.9×10^{13} Jones at 0 N to 3.5×10^{13} Jones at 73.7 N by 3.8×. So, the piezo-phototronic effect can promote the considerable and desired enhancement for the performance. Likewise, responsivity and detectivity for ZnO/CuO/Au devices displayed a monotonous growing trend with the increase of external pressure. The maximums of responsivity and detectivity were obtained as 0.81 mA W^{-1} and 3.3×10^{13} Jones respectively under pressure of

Table 1. Comparison of different ZnO-based devices with pyro-phototronic or piezo-phototronic effect.

Device	Wavelength [nm]	τ_r/τ_d	R [A W^{-1}]	D^* [Jones]	Power density	Voltage [V]	Ref.
ZnO/GaN	352	0.1 s	0.34	4.25×10^{10}	5–20 mW cm^{-2}	0	[40]
V$_2$O$_5$/ZnO	365	4/16 µs	4.4×10^{-3}	7.32×10^{13}	1–4 mW cm^{-2}	0	[42]
ZnO/MeOTAD	365	0.16/0.20s	8×10^{-4}	4.2×10^{9}	1.0 mW cm^{-2}	0	[43]
ZnO/Si	325/442/633/785	0.4/0.7 ms	1.79×10^{-2}	2.94×10^{9}	0.6–97 mW cm^{-2}	0	[35]
Si/ZnO/PEDOT: PSS	405/648	5.40/24.4ms	1.2×10^{-2}	1.8×10^{10}	0.31-39.63 mW cm^{-2}	−2	[39]
Si/SnOx/ZnO	405/650	3/2 µs	36.7	1.5×10^{11}	36 mW cm^{-2}	0	[44]
Cl:ZnO/PEDOT:PSS	365	28/23 ms	2.33×10^{-3}	1.54×10^{10}	0.3 mW cm^{-2}	0	[17]
NiO/ZnO	365	2.4 s			20 mW cm^{-2}	3	[45]
BFO/Au /ZnO	360–1060				3–650 mW cm^{-2}	0	[46]
ZnO/Si	1064	15/21 µs	0.16	8.8×10^{11}	26 mW cm^{-2}	−2	[47]
ZnO/CuO/Au	325	18/12 ms	8.1×10^{-5}	3.3×10^{13}	140 nW cm^{-2}	0	This work

73.7 N (Figure 4b). Detectivity increased by 2.5× from 1.3×10^{13} to 3.3×10^{13} Jones. This enhancement can be attributed to the comprehensive effect of LSPR, pyro-phototronic and piezo-phototronic. The enhancement by the comprehensive effect was a little less than that of individual piezo-phototronic. The reason was that there was larger detectivity in ZnO/CuO/Au devices under pressure of 0 N for the LSPR-inspired pyro-phototronic effect compared with ZnO/CuO devices without LSPR-inspired pyro-phototronic effect. On the other hand, piezo-phototronic effect may play a more important part than LSPR-inspired pyro-phototronic effect, and the comprehensive effect was not probably simple addition of LSPR-inspired pyro-phototronic effect and piezo-phototronic effect. The relative change of responsivity was defined as $\Delta R/R_0 = (R - R_0)/R_0$ to illustrate enhancement of coupled LSPR-inspired pyro-phototronic and piezo-phototronic effect, where R and R_0 were the responsivity under pressure and pressure free conditions, respectively. It was clear that $\Delta R/R_0$ for coupled LSPR-inspired pyro-phototronic effect and piezo-phototronic effect grew up as the external pressure rose up. The $\Delta R/R_0$ for a ZnO/CuO device and a ZnO/CuO/Au device also exhibited a similar law of increase, rising as much as 753% and 504% (Figure 4c). It demonstrated the great improvement of piezo-phototronic effect for performance again. More importantly, it can be found that $\Delta R/R_0$ for coupled LSPR-inspired pyro-phototronic effect and piezo-phototronic effect was much larger than that of individual piezo-phototronic effect in a ZnO/CuO device or a ZnO/CuO/Au device, running up to as much as 1700% (Figure 4c). Thus, the coupled LSPR-inspired pyro-phototronic effect and piezo-phototronic effect can dramatically improve the responsivity in the ZnO/CuO/Au device. Additionally, the rise time and fall time reduced from 114/75 ms of a ZnO/CuO device to 18/12 ms of a ZnO/CuO/Au device under pressure of 64.7 N (Figure 4d). The coupled effect was also used to detect visible light. However, it achieved extremely low responsivity, compared to detecting UV light (Figure S9, Supporting Information). The devices displayed a little response to 450 nm light even though the power density reached to 128 µW cm^{-2}, and applying external pressure had little influence on the responsivity but can shorten the response and recovery time noticeably owing to the enhancement of pyro-phototronic effect. The rise time/fall time was reduced ≈ten times under 64.7 N pressure. However, compared to 325 nm UV light with low power density of 140 nW cm^{-2}, the photoresponse for 450 nm light was such weak that the responsivity was only ≈1% of responsivity for 325 nm light (140 nW cm^{-2}) even though the power density increased by three orders of magnitude. The devices showed no response to 550 nm (1.22 mW cm^{-2}) and 660 nm light (1.31 mW cm^{-2}).

Furthermore, the spectral photoresponse analysis was obtained to show the coupled effect of LSPR-inspired pyro-phototronic effect and piezo-phototronic effect on range of detection signal, where the responsivity varied in the spectral range from 325 to 1030 nm. The major peak in the UV region suggested that ZnO/CuO/Au devices were extremely sensitive to ultraviolet.[41] Though there was a small responsivity peak at 450 nm, UV/visible rejection ratio was ≈160. Moreover, by applying external pressure of 25.8 N, the major responsivity peak was still in UV region, which indicated that the coupled effect exhibited little effect on the range of detection signal except for the response intensity. Therefore, the results from spectral photoresponse analysis demonstrated the as-prepared photodetectors were visible-blind self-powered photodetectors for UV detection (Figure S10, Supporting Information). **Table 1** exhibited the comparison of the as-fabricated photodetectors with recent ZnO-based photodetectors with piezo-phototronic and/or pyro-phototronic effect on photoresponse parameters. The devices in this work had a tremendous advantage in their ability to detect weak signals as the detectivity was considerable high.

According to previous analysis of our results, it can be found that LSPR, pyro-phototronic, and piezo-phototronic effect have been well coupled in the ZnO/CuO/Au devices and played a key role in enhancing the performance of photodetection. Then, energy band diagrams were used to further explain the tuning role of coupled LSPR-inspired pyro-phototronic effect and piezo-phototronic effect. The valence band and conduction band of ZnO (electron affinity ≈4.2 eV) were −7.71 and −4.35 eV versus vacuum. The valence band and conduction band of CuO were −5.47 and −4.0 eV versus vacuum. In the ZnO/CuO devices, it generated photocurrent mainly due to a built-in potential in p-n junction of ZnO/CuO which separated the photogenerated electron-hole pairs and generated the
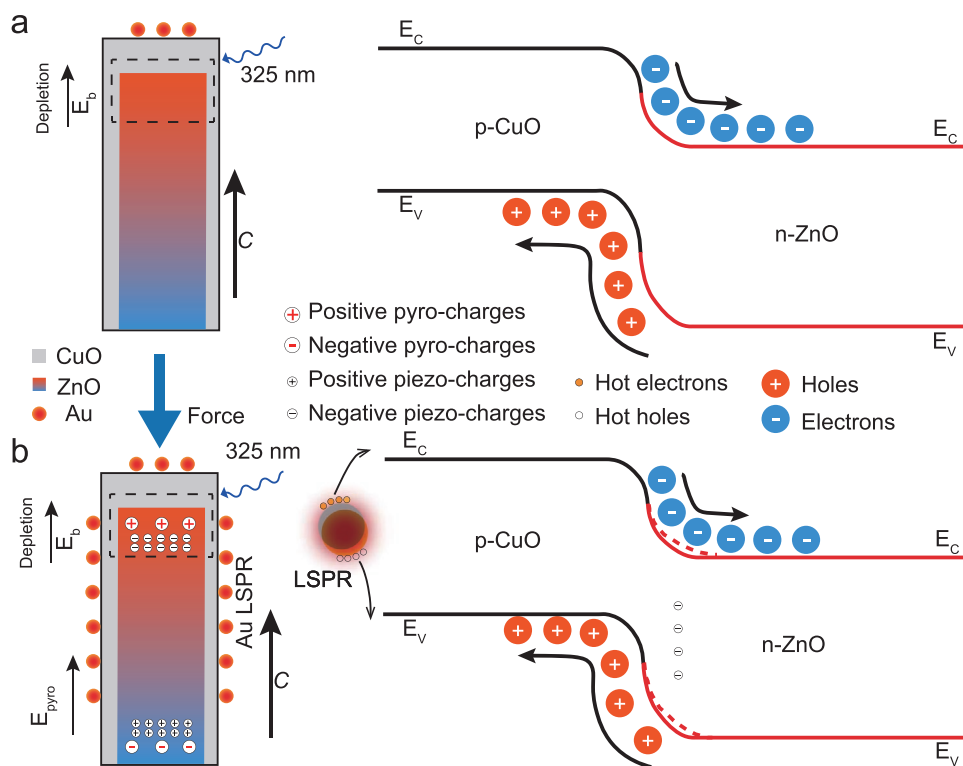
**ADVANCED
SCIENCE NEWS**

www.advancedsciencenews.com

**ADVANCED
OPTICAL
MATERIALS**

www.advopticalmat.de

Figure 5. Coupled mechanism of LSPR, pyro-phototronic and piezo-phototronic. a) Energy band diagrams of a ZnO/CuO device without external pressure under 325 nm illumination. b) Energy band diagrams of a ZnO/CuO device with external pressure under 325 nm illumination.

photovoltage as external pressure was not applied (**Figure 5**a). Furthermore, ZnO/CuO devices did not display pyroelectric current, because the UV light (140 nW m^{-2}) was so weak that small temperature variation was generated in ZnO nanorods. In ZnO/CuO/Au devices, the Au NPs were considered to have little effect on the energy band, thus, the origin energy band (solid line) was the same as that of ZnO/CuO devices (Figure 5b). The coupled LSPR-inspired pyro-phototronic effect and piezo-phototronic effect produced at the moment of turning on/off the 325 nm laser. This comprehensive effect was attributed to two processes. On the one hand, the pressure was applied on the device and piezoelectric polarity charges distributed in ZnO along the *c*-axis (Figure 5b). The negative piezo-charges generated at the n-ZnO/p-CuO interface resulting in an upward bending of the local energy band diagram at the n-ZnO/p-CuO interface (dashed line), and the negative piezo-charges can draw holes in p-CuO toward and repel electrons in n-ZnO away from the interface.[48] Consequently, the electron depletion region at the n-ZnO side expanded, enhancing the production and separation of the photo-generated electron-hole pairs.[39] Moreover, plasmonic hot electrons and hot holes were involved into photocurrent (Figure 5b). In a word, photoresponse of the ZnO/CuO/Au devices can be improved greatly. On the other hand, LSPR induced by Au NPs on the surface of CuO produced transient thermal power to make temperature change quickly at the moment of light illumination (in 300 ps[49,50]), which led to positive pyroelectric charges at n-ZnO side and contributed to producing pyroelectric current. Hence, appearance of pyroelectric current decreased response time of the photodetectors dramatically and increased responsivity and

detectivity of the photodetectors largely. Besides, plasmonic hot electrons can boost or generate the internal photoemission in photodetectors and contributed to photocurrent leading to improvement of the photo-response intensity.[49]

We have proposed a strategy to couple LSPR, pyro-phototronic, piezo-phototronic effect in a self-powered photo-detector based on ZnO/CuO core-shell nanorods decorated with Au NPs, and systematically investigated and thoroughly analyzed the interaction among these mechanisms under weak UV radiation. First, LSPR induced by Au NPs made pyro-phototronic operate, which was named LSPR-inspired pyro-phototronic effect and can enhance the performance of photodetectors. Piezo-phototronic can also promote improvement of the photodetectors. More importantly, coupled LSPR-inspired pyro-phototronic and piezo-phototronic effect made the performance of photodetectors more excellent. Thus, to couple LSPR, pyro-phototronic, piezo-phototronic effect was an effective method to improve a photodetector as detecting weak ultraviolet. Detection of ultraviolet with low power density (140 nW cm^{-2}) was achieved in the self-powered photo-detector. It was a very crucial merit for photodetectors to be applied in some fields such as optical communication and strain imaging. Moreover, this approach was also suitable for other pyroelectric and piezoelectric semiconductor-material combinations, including visible and/or infrared-sensitive materials, and thus the range of practical applications was extended. Plasmonic hot carrier generation and other energy transfer mechanisms were caught much attention and used to improve photodetector performance.[49,51–53] However, in the coupled LSPR-inspired pyro-phototronic and piezo-phototronic

effect, more energy utilization efficiency of plasmons was realized for involving plasmonic heat effect, which was the cornerstone of detecting weak UV for the self-powered ZnO/CuO/Au photodetector. The performance of photodetectors enhanced by coupling LSPR-inspired pyro-phototronic effect and piezo-phototronic effect have been evaluated by $\Delta R/R_0$ that increased by 1700%. Response time can be decreased by this comprehensive effect. Therefore, coupled LSPR-inspired pyro-phototronic and piezo-phototronic effect demonstrated synergistic properties and greater potential in improving performance of a photodetector. Additionally, the array structure of nanorods enabled the photodetector to trap light more efficiently. And the self-powered photodetection was beneficial to device integration, avoiding extra cost and energy consumption.[54–56]

3. Conclusion

In summary, we successfully combined LSPR, pyro-phototronic, and piezo-phototronic effect in a self-powered photodetector integrated with ZnO/CuO core-shell nanorods decorated by Au NPs. The performance of photodetectors was enhanced dramatically by this comprehensive effect that coupling LSPR-inspired pyro-phototronic and piezo-phototronic effect when detecting weak ultraviolet radiation with power density as low as 140 nW cm^{-2}. $\Delta R/R_0$ of ZnO/CuO/Au increased by 1700%. Rise time and fall time reduced from 114/75 ms of a ZnO/CuO device to 18/12 ms of a ZnO/CuO/Au device under pressure of 64.7 N. The maximums of responsivity and detectivity were obtained as 0.81 mA W^{-1} and 3.3×10^{13} Jones respectively under pressure of 73.7 N. Meanwhile, LSPR-inspired pyro-phototronic effect and piezo-phototronic effect was also investigated and the results showed that individual pyro-phototronic effect inspired by LSPR and individual piezo-phototronic effect can enhance the performance of photodetectors. However, coupled LSPR-inspired pyro-phototronic and piezo-phototronic effect made greater improvement than the individual effect in performance of photodetectors. This work may provide in-depth cognition on LSPR, pyro-phototronic and piezo-phototronic effect that affected performance of ZnO/CuO/Au photodetectors. We believe that this work probably is a cornerstone to design high-performance photodetectors using other nanomaterial systems as well.

4. Experimental Section

Material Preparation: First, ZnO seed layer was deposited by Magnetron Sputtering Machine (Denton Discovery 635) on FTO glasses at room temperature. Second, a simple hydrothermal method by modifying the reported method[18] was used to grow ZnO nanorods. And then, ZnO nanorods was immersed in a solution addition of 4 mL NaOH (0.1 м), 4 mL Cu(NO$_3$)$_2$ (0.1 м), 4 mL NH$_4$·H$_2$O (5 м), and 40 mL H$_2$O and heated at 90 °C for 30 min to deposit CuO on the surface of ZnO. Finally, Au NPs were attached on surface of CuO by 108 Auto Cressington sputter coater with 20 mA current for 20 s.

Device Fabrication: The materials were covered with FTO top electrodes and wires were connected to the top and bottom FTO electrodes using silver paste.

Material Characterization: Detailed microscopic structures of ZnO, ZnO/CuO, and ZnO/CuO/Au were imaged using scanning electron microscope (Hitachi SU8020 and Nova 450), transmission electron microscope, and high-resolution transmission electron microscope (Tecnai G^2 F20) as well as corresponding energy dispersive spectrometer at room temperature. X ray diffractometer (PANalytical X'Pert) with Cu K$_\alpha$ radiation, PL spectra, and Raman spectra (LabRAM HR Evolution, Horiba) were used to analyze crystal and elementary composition at room temperature. Absorption spectra was obtained using Shimadzu UV3600.

Optical and Electrical Measurements: Monochromatic 325 nm lasers (KIMMON IK330IR-G) and LED light (MLED4-4, 365 to 1030 nm) were used as light sources. The power density for devices was measured by digital power meters (Thorlab PM100D). A Keithley 4200 semiconductor analyzer, a LeCroy oscilloscope and a Keithley 6517B high resistance electrometer were used to obtain the I–V characteristics and I–t characteristics for the photodetectors.

Supporting Information

Supporting Information is available from the Wiley Online Library or from the author.

Conflict of Interest

The authors declare no conflict of interest.

Data Availability Statement

Research data are not shared.

[1] D. Guo, Y. Su, H. Shi, P. Li, N. Zhao, J. Ye, S. Wang, A. Liu, Z. Chen, C. Li, W. Tang, *ACS Nano* **2018**, *12*, 12827.

[2] Y. Wang, L. Zhu, Y. Feng, Z. Wang, Z. L. Wang, *Adv. Funct. Mater.* **2018**, *29*, 1807111.

[3] J. Meng, H. Li, L. Zhao, J. Lu, C. Pan, Y. Zhang, Z. Li, *Nano Lett.* **2020**, *20*, 4968.

[4] J. Li, X. Liu, L. Tan, Y. Liang, Z. Cui, X. Yang, S. Zhu, Z. Li, Y. Zheng, K. W. K. Yeung, X. Wang, S. Wu, *Small Methods* **2019**, *3*, 1900048.

[5] B. D. Boruah, *Nanoscale Adv.* **2019**, *1*, 2059.

[6] Y. K. Su, S. M. Peng, L. W. Ji, C. Z. Wu, W. B. Cheng, C. H. Liu, *Langmuir* **2010**, *26*, 603.

[7] S. Jeon, S. Ahn, I. Song, C. J. Kim, U. Chung, E. Lee, I. Yoo, A. Nathan, S. Lee, K. Ghaffarzadeh, J. Robertson, K. Kim, *Nat. Mater.* **2012**, *11*, 301.

[8] Z. L. Wang, *Adv. Mater.* **2007**, *19*, 889.

[9] Z. Wang, R. Yu, C. Pan, Z. Li, J. Yang, F. Yi, Z. L. Wang, *Nat. Commun.* **2015**, *6*, 8401.

[10] J. Meng, Q. Li, J. Huang, Z. Li, *Nanoscale* **2021**, *13*, 17101.

[11] X. Han, W. Du, R. Yu, C. Pan, Z. L. Wang, *Adv. Mater.* **2015**, *27*, 7963.

[12] C. Liu, M. Peng, A. Yu, J. Liu, M. Song, Y. Zhang, J. Zhai, *Nano Energy* **2016**, *26*, 417.

[13] Z. Wang, R. Yu, C. Pan, Y. Liu, Y. Ding, Z. L. Wang, *Adv. Mater.* **2015**, *27*, 1553.

[14] J. Meng, Z. Li, *Adv. Mater.* **2020**, *32*, 2000130.

[15] S. Podder, B. Basumatary, D. Gogoi, J. Bora, A. R. Pal, *Appl. Surf. Sci.* **2021**, *537*, 147893.

[16] D. You, C. Xu, W. Zhang, J. Zhao, F. Qin, Z. Shi, *Nano Energy* **2019**, *62*, 310.

[17] B. B. Deka, M. S. Naidu, S. Nandi, A. Misra, *Nanoscale* **2018**, *10*, 3451.

[18] W. Peng, X. Wang, R. Yu, Y. Dai, H. Zou, A. C. Wang, Y. He, Z. L. Wang, *Adv. Mater.* **2017**, *29*, 1606698.

[19] Y. Ji, K. Zhang, Z. L. Wang, Y. Yang, *Energ. Environ. Sci.* **2019**, *12*, 1231.

[20] K. Song, R. Zhao, Z. L. Wang, Y. Yang, *Adv. Mater.* **2019**, *31*, 1902831.

[21] Y. Zhu, B. Wang, C. Deng, Y. Wang, X. Wang, *Nano Energy* **2021**, *83*, 105801.

[22] G. Yu, J. Qian, P. Zhang, B. Zhang, W. Zhang, W. Yan, G. Liu, *Nat. Commun.* **2019**, *10*, 4912.

[23] X. Chen, Y. Chen, M. Yan, M. Qiu, *ACS Nano* **2012**, *6*, 2550.

[24] A. O. Govorov, H. H. Richardson, *Nano Today* **2007**, *2*, 30.

[25] Q. Li, J. Meng, J. Huang, Z. Li, *Adv. Funct. Mater.* **2021**, 2108903.

[26] B. Deka Boruah, A. Misra, *ACS Appl. Mater. Interfaces* **2016**, *8*, 18182.

[27] T. Dixit, I. A. Palani, V. Singh, *J. Phys. Chem. C* **2017**, *121*, 3540.

[28] Z. Liao, H. Zhang, Y. Zhou, J. Xu, J. Zhang, D. Yu, *Phys. Lett. A* **2008**, *372*, 4505.

[29] J. Richters, T. Voss, L. Wischmeier, I. Rückmann, J. Gutowski, *Appl. Phys. Lett.* **2008**, *92*, 011103.

[30] L. Shi, Y. Xu, S. Hark, Y. Liu, S. Wang, L. Peng, K. Wong, Q. Li, *Nano Lett.* **2007**, *7*, 3559.

[31] J. Li, S. K. Cushing, F. Meng, T. R. Senty, A. D. Bristow, N. Wu, *Nat. Photonics* **2015**, *9*, 601.

[32] S. Link, M. A. El-Sayed, *J. Phys. Chem. B* **1999**, *103*, 8410.

[33] S. Link, Z. L. Wang, M. A. El-Sayed, *J. Phys. Chem. B* **1999**, *103*, 3529.

[34] J. Dong, Z. Wang, X. Wang, Z. L. Wang, *Nano Today* **2019**, *29*, 100798.

[35] Y. Zhang, M. Hu, Z. Wang, *Nano Energy* **2020**, *71*, 104630.

[36] Y. Zhang, F. Zhang, Y. Xu, W. Huang, L. Wu, Z. Dong, Y. Zhang, B. Dong, X. Zhang, H. Zhang, *Small Methods* **2019**, *3*, 1900349.

[37] C. Wu, C. He, D. Guo, F. Zhang, P. Li, S. Wang, A. Liu, F. Wu, W. Tang, *Mater. Today Phys.* **2020**, *12*, 100193.

[38] F. Yan, Z. Wei, X. Wei, Q. Lv, W. Zhu, K. Wang, *Small Methods* **2018**, *2*, 1700349.

[39] F. Li, W. Peng, Z. Pan, Y. He, *Nano Energy* **2018**, *48*, 27.

[40] D. J. Lee, S. R. Ryu, G. M. Kumar, H. D. Cho, D. Y. Kim, P. Ilanchezhiyan, *Appl. Surf. Sci.* **2021**, *558*, 149896.

[41] B. D. Boruah, S. N. Majji, A. Misra, *Nanoscale* **2017**, *9*, 4536.

[42] M. Kumar, M. Patel, T. T. Nguyen, J. Kim, J. Yi, *Nanoscale* **2018**, *10*, 6928.

[43] Y. Shen, X. Yan, H. Si, P. Lin, Y. Liu, Y. Sun, Y. Zhang, *ACS Appl. Mater. Interfaces* **2016**, *8*, 6137.

[44] J. P. B. Silva, E. M. F. Vieira, K. Gwozdz, A. Kaim, L. M. Goncalves, J. L. MacManus-Driscoll, R. L. Z. Hoye, M. Pereira, *Nano Energy* **2021**, *89*, 106347.

[45] Y. Luo, B. Yin, H. Zhang, Y. Qiu, J. Lei, Y. Chang, Y. Zhao, J. Ji, L. Hu, *Appl. Surf. Sci.* **2016**, *361*, 157.

[46] Y. Zhang, H. Su, H. Li, Z. Xie, Y. Zhang, Y. Zhou, L. Yang, H. Lu, G. Yuan, H. Zheng, *Nano Energy* **2021**, *85*, 105968.

[47] L. Chen, B. Wang, J. Dong, F. Gao, H. Zheng, M. He, X. Wang, *Nano Energy* **2020**, *78*, 105260.

[48] Z. Zhao, Y. Dai, *Phys. Chem. Chem. Phys.* **2019**, *21*, 9574.

[49] H. Tang, C. Chen, Z. Huang, J. Bright, G. Meng, R. Liu, N. Wu, *J. Chem. Phys.* **2020**, *152*, 220901.

[50] J. W. Stewart, J. H. Vella, W. Li, S. Fan, M. H. Mikkelsen, *Nat. Mater.* **2020**, *19*, 158.

[51] W. Li, J. G. Valentine, *Nanophotonics* **2017**, *6*, 177.

[52] C. de Melo, M. Jullien, Y. Battie, A. E.n Naciri, J. Ghanbaja, F. Montaigne, J. Pierson, F. Rigoni, N. Almqvist, A. Vomiero, S. Migot, F. Mücklich, D. Horwat, *ACS Appl. Mater. Interfaces* **2018**, *10*, 40958.

[53] M. Chen, L. Shao, S. V. Kershaw, H. Yu, J. Wang, A. L. Rogach, N. Zhao, *ACS Nano* **2014**, *8*, 8208.

[54] Y. Zhang, M. Peng, Y. Liu, T. Zhang, Q. Zhu, H. Lei, S. Liu, Y. Tao, L. Li, Z. Wen, X. Sun, *ACS Appl. Mater. Interfaces* **2020**, *12*, 19384.

[55] Z. Zhang, Y. Ning, X. Fang, *J. Mater. Chem. C* **2019**, *7*, 223.

[56] Y. Ning, Z. Zhang, F. Teng, X. Fang, *Small* **2018**, *14*, 1703754.